Golgi-Localized Mannanases Sustain Hemicellulose Biosynthesis

Talia Jacobson[1,2], Mair Edwards[1,2], Moni Qiande[1], Madalen Robert[1,3], Julia Moncrieff[1], Cătălin Voiniciuc[1,2,3*]

[1]Department of Horticultural Sciences, University of Florida, Gainesville, FL 32611, USA

[2]Plant Molecular and Cellular Biology Graduate Program, University of Florida, Gainesville, FL 32609, USA

[3]Independent Junior Research Group–Designer Glycans, Leibniz Institute of Plant Biochemistry, 06120 Halle (Saale), Germany

*** Corresponding Author:** Cătălin Voiniciuc

Email: cvoiniciuc@ufl.edu

Classification: Biological Sciences, Biochemistry

This PDF file includes:

Summary (147 words)
Introduction (798 words)
Materials and Methods (799 words)
Results (1927 words)
Discussion (1236 words)
TOTAL: 4907

References
Fig. 1 to 5 (all in color)

Summary

- Mannans with β-1,4-linked backbones are common cell wall components of algae and land plants. Prior challenges to enhance β-mannan content in plants point to unclear metabolic bottlenecks and the potential for hidden biosynthetic players.
- Endo-β-MANNANASEs (MANs) are the main glycosyl hydrolases that mobilize extracellular β-mannans during seed germination. However, we found that Arabidopsis *man2 man5* seeds resemble β-mannan biosynthetic mutants. CELLULOSE SYNTHASE-LIKE A (CSLA) overexpression restored β-mannan synthesis in the *man* double mutant and increased the distribution of crystalline polymers, but impaired the release of other mucilaginous polysaccharides.
- Using yeast synthetic biology, we dissected the functional interplay of MAN enzymes with CSLAs. Intracellular MAN2 and MAN5 reduced the quantity of insoluble β-mannan but elevated the content of water-soluble carbohydrates.
- We propose that Arabidopsis MAN2/5, and orthologous crop enzymes with a transmembrane domain, sustain hemicellulose production in the Golgi apparatus by cleaving insoluble β-mannan polymers into hydrophilic counterparts.

Keywords: plant cell wall, hemicellulose, polysaccharide biosynthesis, glycosyl hydrolases, synthetic biology

Introduction

Among carbohydrate-active enzymes, glycosyl transferase (GT) and glycosyl hydrolase (GH) enzymes generally play antagonistic roles on plant cell wall polysaccharides. Hemicelluloses can cross-link cellulose microfibrils and interact with pectin domains to shape plant biology, and to define the structure of traits, dietary fibers, materials, and chemical feedstocks for industrial applications. The *Arabidopsis thaliana* (hereafter Arabidopsis) seed coat epidermal cells offer an excellent genetic model system to untangle cell wall polysaccharide biosynthesis and function. Upon contact with water, dry seeds release copious amounts of mucilaginous polysaccharides (Voiniciuc *et al.*, 2015c) with smaller amounts of hemicelluloses such as branched β-mannans (Voiniciuc *et al.*, 2015b) and crystalline cellulose (Griffiths *et al.*, 2015). Plant β-mannan backbones are defined by their β-1,4-linked mannose (Man) residues (Voiniciuc, 2022), but can also contain β-1,4-glucose (Glc). In Arabidopsis mucilage galactoglucomannan (GGM), the Man units are substituted with single α-1,6-linked galactosyl (Gal) residues (Voiniciuc *et al.*, 2015b; Yu *et al.*, 2018), or β-1,2-Gal-α-1,6-Gal disaccharides (Yu *et al.*, 2022). Highly branched GGM contributes to mucilage density and crystalline cellulose deposition (Voiniciuc *et al.*, 2015b), while another hemicellulose, branched xylan, is important for the adherence of pectic rhamnogalacturonan-I (~90% of Arabidopsis mucilage) to the seed surface (Voiniciuc *et al.*, 2015a; Ralet *et al.*, 2016). Other seed-extracted galactomannans (e.g. guar gum and locust bean gum) are frequently added as thickening agents, stabilizers, and emulsifiers in numerous food and household products, or serve as dietary fiber supplements to control appetite and reduce blood Glc levels in patients with type 2 diabetes (Juhász *et al.*, 2023).

Since their backbone and branches are composed entirely of hexose sugars (Scheller & Ulvskov, 2010), plant mannans have desirable properties for a circular bioeconomy and could support the bioengineering of new products or sustainable feedstocks for biomanufacturing (Voiniciuc, 2022, 2023; Jacobson *et al.*, 2024). Despite long-standing demands to elevate hexose sugar content in lignocellulosic biomass (Pauly & Keegstra, 2008), β-mannan content has been challenging to elevate in plants. For instance, seed-specific expression of a guar mannan synthase in the legume *Medicago*

77 *truncatula* severely disrupted metabolism and unexpectedly decreased galactomannan
78 levels (Naoumkina *et al.*, 2008).

79 As recently reviewed (Voiniciuc, 2022), β-mannan biosynthesis is orchestrated by
80 several classes of Golgi-localized glycosyl transferase (GTs) with a suite of secreted
81 glycosyl hydrolases (GHs) expected to modify polysaccharides after their deposition in the
82 cell wall. CELLULOSE SYNTHASE-LIKE A2 (AtCSLA2) is the chief catalyst for β-
83 mannan elongation in the Arabidopsis seed coat (Yu *et al.*, 2014). During mucilage GGM
84 elongation, MUCILAGE-RELATED10 (AtMUCI10 also known as AtMAGT1) decorates
85 Man residues with single α-1,6-Gal side chains (Voiniciuc *et al.*, 2015b; Yu *et al.*, 2018),
86 which can be further substituted with β-1,2-Gal residues by AtMBGT1 (Yu *et al.*, 2022).
87 Plant mannans are often galactosylated (Scheller & Ulvskov, 2010) or acetylated (Zhong
88 *et al.*, 2019) because *in vitro* assays show that β-mannan oligosaccharides crystallize as
89 they elongate (Grimaud *et al.*, 2019). In the yeast *Pichia pastoris* (hereafter *Pichia*),
90 MANNAN-SYNTHESIS RELATED1 (AtMSR1) acts as a co-factor that enables
91 AtCSLA2 to produce glucomannan instead of relative pure mannan (Voiniciuc *et al.*,
92 2019). Since *Amorphophallus konjac* AkCSLA3 can produce glucomannan even without
93 MSR1 in yeast, it has been used to investigate the protein regions important for substrate
94 specificity (Robert *et al.*, 2021), to illuminate the localization and bottlenecks for
95 hemicellulose biosynthesis (Grieß-Osowski *et al.*, 2025).

96 Once β-mannans are deposited in the cell wall, endo-β-1,4-MANNANASES
97 (MANs) become the chief catalysts for the backbone modification and degradation. While
98 the biological roles of different mannan structures remains remain ambiguous (Boerjan *et*
99 *al.*, 2024; Guevara-Rozo *et al.*, 2025), MANs are involved in wall softening and
100 carbohydrate release during plant development (Rodríguez-Gacio *et al.*, 2012). MAN
101 hydrolytic activity increases in a wide range of plant species during seed germination,
102 presumably to mobilize carbon reserves and to promote growth (Downie *et al.*, 1997;
103 Nonogaki *et al.*, 2000; Wang *et al.*, 2005; Iglesias-Fernández *et al.*, 2011, 2020; De Farias
104 *et al.*, 2015; Carrillo-Barral *et al.*, 2018). Four of the seven *Arabidopsis MAN* genes are
105 expressed in dry seeds and three different single mutants (*man5*, *man6,* and *man7*, but not

106 *man2*) decreased or delayed germination (Iglesias-Fernández *et al.*, 2011). Mannan
107 oligosaccharides released by AtMAN6 are proposed to activate signaling for xylem
108 thickening, while AtMAN3 and AtMAN7 are induced by cadmium to increase apoplastic
109 Man and promote heavy metal tolerance (Chen *et al.*, 2015; Wu *et al.*, 2023; Zhang *et al.*,
110 2024). Some MANs also have transglycosylation activity to essentially 'cut-and-paste'
111 polymers, e.g. for fruit ripening (Schröder *et al.*, 2009). Intriguingly, some *MANs* are co-
112 expressed with *CSLAs* during seed development in Arabidopsis (Voiniciuc, 2022) and in
113 crops like coffee (Joët *et al.*, 2014), but their impact on hemicellulose accumulation
114 remains unknown (Voiniciuc, 2022). Here, we apply plant and yeast bioengineering
115 strategies to demonstrate that Arabidopsis MAN2 and MAN5 have non-canonical roles in
116 the synthesis of soluble β-mannans.

117 **Materials and Methods**

118 The following sections describe the major materials and methods, with additional details
119 for plant cultivation conditions, DNA construct assembly, yeast growth, biochemical
120 analyses, cytometry and microscopy in the supplemental information (Methods **S1)**.
121

122 **Genetic Materials and Analyses**

123 Arabidopsis T-DNA insertion mutant seeds were obtained from the ABRC or
124 NASC stock centers, *man2-1* (SALK_126628c.20.a), *man2-2* (SALK_016450), *man5-1*
125 (707G06.01.a), *man5-2* (SALK_015220), *man5-3* (SALK_068367), *man2-1 man5-1*
126 (2716/1a1.01), *muci10-1* (SALK_061576), and *csla2-3* (SALK_149092). *Agrobacterium*-
127 mediated transformations of *Arabidopsis* plants, and transient assays in *Nicotiana*
128 *benthamiana* leaves were conducted using established protocols (Yang *et al.*, 2022). For
129 co-localization experiments, plasmid DNA for the Golgi yellow fluorescent protein (YFP)
130 marker G-yk, previously validated for Arabidopsis (Nelson *et al.*, 2007), was obtained from
131 ABRC (CD3-965).

132 Table **S1** lists the genotyping primers for the plant Touch-and-Go Method
133 (Berendzen *et al.*, 2005) or for bacteria or yeast colony polymerase chain reaction (PCR).
134 Cloning was mainly performed Golden Gate assembly (Engler *et al.*, 2014; Marillonnet &

135 Grützner, 2020), or NEB HiFi cloning (Table **S2**), as noted in Methods **S1**. Transcript
136 levels in mature green siliques were analyzed using prior methods (Voiniciuc *et al.*, 2015b)
137 and normalized to the geometric mean of two housekeeping genes (Table **S1**).

138 **Biochemical Analysis of Mucilage and Yeast Cell Wall Fractions**

139 Total mucilage was extracted for monosaccharide profiling via High-Performance
140 Anion-Exchange Chromatography with Pulsed Amperometric Detection (HPAEC-PAD)
141 as specified by (Voiniciuc *et al.*, 2015b; Voiniciuc & Günl, 2016), using an established
142 Metrohm HPAEC-PAD system and eluent gradient (Robert *et al.*, 2021). *Pichia* alkaline-
143 insoluble (AKI) polymers were isolated as previously described (Robert *et al.*, 2021),
144 followed by the separation of alkaline-soluble fractions (Voiniciuc *et al.*, 2019). Water-
145 soluble glycans were extracted from *Pichia* cells as previously described (Cocuron *et al.*,
146 2007) with an incubation step in 70% ethanol for 5 min and a subsequent incubation in
147 water for 5 min at 100 C without Triton X-100. After centrifugation, the supernatant was
148 removed, hydrolyzed, and injected for HPAEC-PAD analysis. The remaining AKI was
149 incubated in NaOH for 90 min followed by hydrolysis. Water-soluble glycans from
150 Arabidopsis dry seeds were analyzed in a similar manner. Seeds were first ground and then
151 incubated in ethanol and then water. The water-soluble and alcohol-insoluble residue (AIR)
152 fractions were then hydrolyzed with trifluoroacetic acid and analyzed via HPAEC-PAD.

153 **Light Microscopy of Plant Materials and Yeast**

154 Seed mucilage area was stained with ruthenium red (RR) (Voiniciuc *et al.*, 2015b)
155 and quantified using an AXIO Vert A1 or a stereoscope equipped with an Axiocam 208
156 color camera or a 202 monochrome camera (all from Zeiss). Seed birefringence in water
157 was captured with an adjustable polarizer/analyzer module, and intensity plots were
158 generated as previously described (Voiniciuc *et al.*, 2016). Confocal images were captured
159 on a Leica Stellaris 8 at the University of Florida Interdisciplinary Center for
160 Biotechnology Research (UF/ICBR) Cytometry Core Facility (RRID: SCR_019119).
161 Unless otherwise noted in figure legends, the 20x (0.75 NA, numerical aperture) objective
162 was used with additional zoom in the Leica LAS X software. Calcofluor white (CF)

163 staining of seeds (Voiniciuc *et al.*, 2015b) or yeast (Robert *et al.*, 2021) was performed
164 using 0.01% Fluorescent Brightener 28 (Sigma Aldrich). Mucilage immunolabeling was
165 followed an established protocol (Voiniciuc, 2017), using four monoclonal antibodies
166 CCRC-M36, CCRC-M70, CCRC-M75, and CCRC-M170 (CarboSource Services,
167 University of Georgia) and a goat anti-mouse Alexa Fluor 488 secondary antibody
168 (ThermoFisher Scientific, A28175). Confocal images were acquired with the following
169 (Excitation | Emission) wavelengths: CF or turquoise protein fluorescence (405 nm | 450-
170 470 nm), green or yellow protein fluorescence (500 nm | 505-550 nm), red fluorescence
171 (550 nm | 600-640 nm). All plant and *Pichia* images were processed and analyzed with the
172 Fiji distribution of ImageJ (Schindelin *et al.*, 2012).

173 **Application of MannanTrack Probe in Yeast**

174 The MannanTrack probe used here is corresponds to + pFDH1:PaCBM35:pmScarlet-I-2A-
175 pSmTq2(stop)ScCYC1tt αMF-PaCBM35-mScarlet-P2A-mTurquoise2 and is introduced
176 in the Results section, and is part of an upcoming collection of genetically encoded probes
177 for plant mannan synthases (Robert *et al*, manuscript in preparation). This MannanTrack
178 coding sequences were codon optimized for *Pichia pastoris*, synthesized and assembled
179 using Golden Gate cloning in the GoldenPiCS vector BB3rN_14, under the control of the
180 pFDH1 methanol-inducible promoter and the ScCYC1tt transcriptional terminator
181 (Prielhofer *et al.*, 2017) Competent *Pichia* cells harboring the *AkCSLA3-Venus* cassette
182 were transformed with the MannanTrack construct, integrated into the *RGI2* locus. After
183 PCR genotyping and growth in YPM + G medium as previously described (Robert *et al.*,
184 2021), a representative colony was selected and made competent (Lin-Cereghino *et al.*,
185 2005). *MAN* episomal vectors were then introduced into the background. All colonies were
186 verified via PCR genotyping before growth and further analyses specified in **Methods S1**.

187 **Statistical Analyses**

188 Statistically significant changes were identified one-way ANOVA analyses performed in
189 PAST 5 software (Hammer *et al.*, 2001), or using Microsoft Excel's t.test function
190 assuming two-tailed distribution and equal variance of two samples.

Results

man2 man5 Seeds Resemble Mannan-Deficient *csla2* and *muci10* Mutants

We focused on deciphering the roles of *MAN2* and *MAN5* (Fig. **1a**), two closely related paralogs with overlapping expression profiles (Iglesias-Fernández *et al.*, 2011). We obtained an uncharacterized *man2-1 man5-1* double mutant from the GABI-DUPLO collection (Bolle *et al.*, 2013), which targeted unlinked gene pairs in Arabidopsis. Real-time PCR confirmed that single and double mutants significantly reduced the transcript levels of the respective genes in developing siliques, at the stage of mucilage production (Fig. **1b**). The *man2-1 man5-1* seeds had 30% smaller mucilage capsules than the wild type (WT), (Fig. **1c**,**d**), while single *man2/5* mutants were not significantly different. Such defects are observed in several mucilage mutants, including *csla2* (Yu *et al.*, 2014) and *muci10* seeds with arrested β-mannan synthesis (Voiniciuc *et al.*, 2015b). In contrast to the reduced *MAN2* and *MAN5* transcript levels, the expression of *CSLA2* or *MUCI10* was not significantly altered in the *man2 man5* double mutant (Fig. **1b**). Additional insertions in *MAN5* could not be verified (Table **S1**), so we crossed an independent *man2-2* allele to *man5* plants and isolated a novel *man2-2 man5* double mutant, which also had compact mucilage compared to WT, without altering the seed dimensions (Fig. **1c-e**). Consistent with prior *man5* data (Iglesias-Fernández *et al.*, 2011), only 50% of *man2 man5* seeds germinated after 48 h after stratification, compared to 80% of WT seeds (Fig. **2b**). The double mutant seeds had delayed germination across growth batches (Figs. **2b**, **S1c)**, but caught up with WT and *csla2* seeds by 96-120 h.

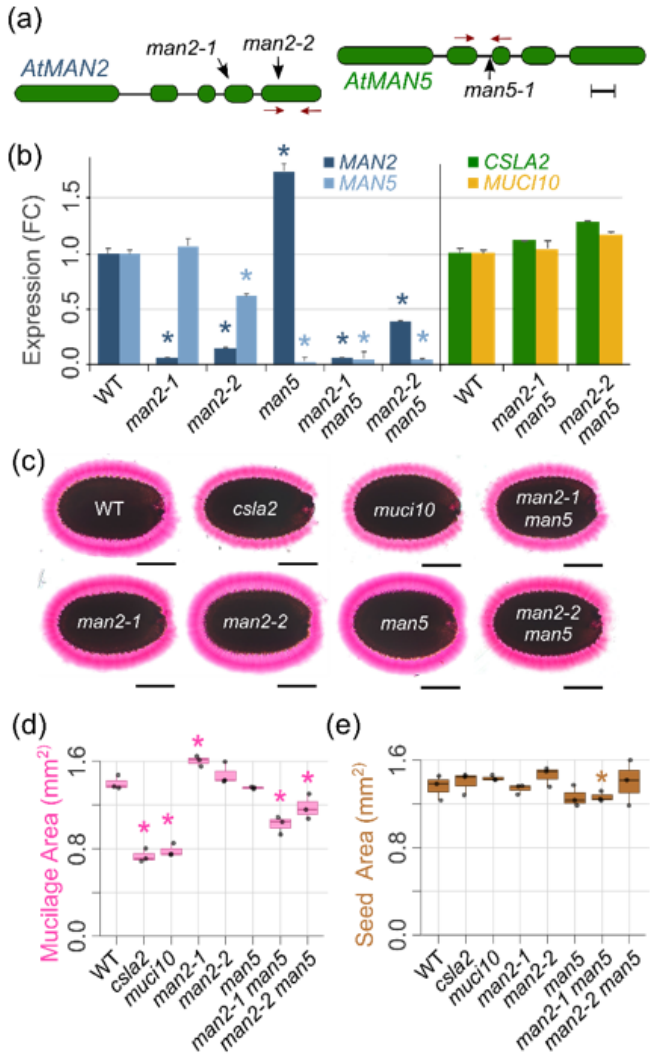

Fig. 1. Mannanase double mutant Arabidopsis seeds have decreased mucilage accumulation. (a) T-DNA insertions in *AtMAN2* and *AtMAN5* genes, showing exon and intron structure. Red arrows indicate positions of primer binding utilized for quantitative PCR (Scale bar, 200 bp). (b) Fold changes in *AtMAN2* and *AtMAN5* or *AtCSLA2* and *AtMUCI10* transcription relative to WT in mature green siliques. Data show mean + SD of three biological replicates normalized to the geometric mean of *UBQ5* and *GAPC1*. Asterisks indicate significant decreases relative to WT (Student's *t* test, $P < 0.01$). (c) Pectin release of WT and mutant seeds stained with RR. (d) Projected mucilage and (e) seed surface area. Data shows mean + SD of three biological replicates (around 20 seeds each). Asterisks indicate significant decreases relative to WT (Student's *t* test, $P < 0.05$). Bars: (c) 200 μm.

To understand why mutations in β-mannan synthases and hydrolases resulted in similar staining defects, despite their antagonistic biochemical activities, we profiled total mucilage composition with HPAEC-PAD. Compared to *man* single mutants and WT, *man2 man5* mucilage contained significantly less Gal and Man, the most characteristic monosaccharides of branched β-mannans (Fig. **2c**; Table **S3a**). Glc, the third component of GGM, showed similar trends but had a high coefficient of variation because it can be derived from several cell wall polymers as well as starch. Although pectin immunolabeling with CCRC-M36 showed results consistent with the RR staining defects, β-mannan antibodies (M70, M75, or M170) in the CCRC collection (Thorne *et al.*, 2023) could not bind WT or *man2 man5* mucilage (Fig. **S1e**). Nevertheless, *man2 man5* mucilage

phenotypes and chemotypes approached the severity of *csla2* and *muci10*, with up to 50% reductions in Gal and Man compared to WT across multiple growth batches (Figs. **2c**, **3c, S1**). These data are consistent with the participation of *MAN2* and *MAN5* in β-mannan production, rather than its catabolism in the seed coat.

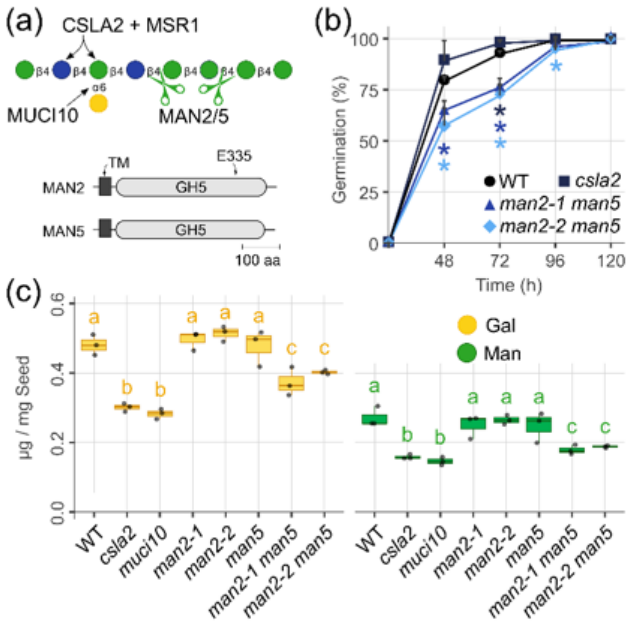

Fig. 2. The *man2 man5* mutant seeds are impaired in β-mannan elongation. (a) Schematic of mucilage mannan biosynthesis and MAN2/5 protein domains. (b) Mean + SD germination rate for three biological replicates. For each time point, asterisks indicate significant decreases relative to WT (Student's *t* test, $P < 0.05$). (c) Absolute monosaccharide levels of three biological replicates. Different letters denote significant changes with one-way ANOVA (Tukey's post-hoc test, $P < 0.01$).

AtCSLA2 Overexpression Rescues *csla2* Defects, but Impairs *man2 man5* Mucilage

Despite the yeast activities described later in the Results section, CSLAs and MANs cDNA sequences (Fig. **S1a,b**) have been difficult to express in plants. In this study, we found that *csla2* mucilage β-mannan deficiency (Table **S3b**) can be rescued with a seed coat-specific *pTBA2:CSLA2* construct, featuring the *TESTA ABUNDANT2* promoter (McGee *et al.*, 2021). The *CSLA2* transgene restored the RR staining of pectin (Fig. **S2a)** and CF staining of cellulosic rays (Fig. **3a**) around *csla2* seeds. In contrast, when introduced in the *man2 man5* background, *pTBA2:CSLA2* led to longer yet disordered rays (Fig. **3a,b**) and a patchy mucilage capsule (Fig. **S2a**). The trends in cellulose staining were supported by imaging of crystalline polymer birefringence under polarized light. The *man2 man5* double mutants had an intermediate reduction of birefringence compared to *csla2* seeds (Fig. **S2b-d**). Although *CSLA2* overexpression in the *man2 man5* seed coat elevated Man and Gal content to nearly WT levels (**Fig. 3c**), it decreased the amount of total

241 extractable mucilage by nearly 60% (Fig. **3d,** Table **S3b**). This was likely due to reduced
242 mucilage release/extraction, rather than impaired secretion, because scanning electron
243 microscopy (SEM) did not reveal major changes in the surface morphology of the mucilage
244 pockets or the columellae (Fig. **S1d**).

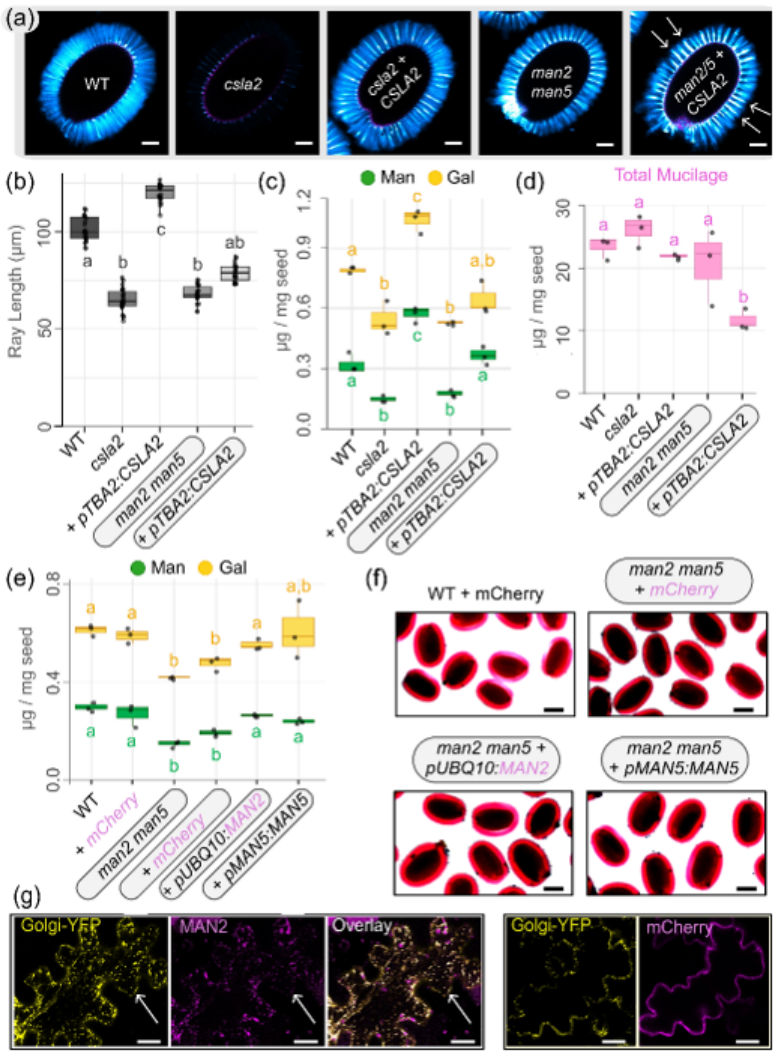

Fig. 3. Golgi-localized MAN enzymes are important for mucilage structure. (a) CF staining of β-glucans in seed mucilage. Arrows mark disordered rays. (b) Length of CF-stained rays. (c) *AtCSLA2* overexpression affects Gal and Man content, and (d) total mucilage release. Biochemical (e) and mucilage RR staining (f) complementation of *man2 man5* by AtMAN gDNA constructs. Different letters denote significant changes with one-way ANOVA (Tukey's post-hoc test, $P < 0.01$). (g) Optical sections of *N. benthamiana* leaves expressing a Golgi-YFP marker and AtMAN2-mCherry or an mCherry control. Arrows mark co-localization. Bars: (a) 100 µm, (f) 200 µm, (g) 30 µm.

245

246 **Non-Canonical MAN2 and MAN5 Localize in the Golgi Apparatus**

247 Unlike most plant and microbial MANs, AtMAN2 and AtMAN5 are predicted to
248 have an N-terminal transmembrane domain instead of a signal peptide (Figs. **2a, S3**).
249 However, determining their subcellular localization *in planta* was not straightforward and
250 required extensive troubleshooting (summarized in Table **S4**). *AtMAN2/5* cDNA sequences

251 did not show any detectable protein expression/function *in planta* using *pTBA2*, the
252 putative *pMAN2* promoter, or the viral *p35S* promoter (Fig. **S1a-d**). Similar vectors worked
253 for fluorescent protein controls and cDNA sequences for other enzymes (e.g. CSLA2), but
254 plant gene expression may require distal or intron-localized enhancers (Vollen *et al.*, 2024),
255 which are difficult to predict. To circumvent these unexpected challenges, we amplified
256 *AtMAN*^{gDNA} genomic sequences for C-terminal *mCherry* fusions driven by the Arabidopsis
257 *UBIQUITIN10* promoter (*pUBQ10)*. At long last, the *MAN2*^{gDNA}*-mCherry* combination
258 showed detectable fluorescence after transient expression in *N. benthamiana*. Unlike the
259 cytosolic mCherry control, MAN2-mCherry co-localized with the known Golgi-YFP
260 marker G-yk (Nelson *et al.*, 2007), in small punctae (Fig. **3g**) and showed similar
261 trajectories (Video **S1**), consistent with roles in mannan biosynthesis**.** Since *MAN5*^{gDNA}-
262 *mCherry* did not show any detectable fluorescence, we cloned an even longer genomic
263 *MAN5* construct that features its putative promoter, native stop codon, and its 3'
264 untranslated region. Eight *pMAN5:MAN5*^{gDNA} and four *pUBQ10:MAN2*^{gDNA}*-mCherry*
265 transformants rescued the *man2 man5* biochemical defects and compact mucilage
266 phenotype (Fig. **3e,f**, Table **S3c**).

267 **Intracellular MAN2 and MAN5 Reduce Insoluble β-Mannan Accumulation in Yeast**

268 *MAN*^{cDNA}*-mCherry* constructs were expressed in a modular *Pichia* platform via an
269 episomal vector compatible with Plant Modular Cloning (MoClo) standards (Grieß-
270 Osowski *et al.*, 2025). AtMAN2 and AtMAN5 proteins were localized in intracellular
271 compartments (Figs. **4b**, **S4d**) and did not alter the glycan composition of WT X-33 cells
272 (Fig. **4a**). While episomal expression of AtMSR1 enhanced glucomannan production in
273 CSLA yeast strains (Fig. **4a**, **S6a**), co-expression of AtMAN2/5 with either AkCSLA3 or
274 AtCSLA2 reduced insoluble β-mannan content by 30–40% (Figs. **4a**, **S4a**). To ensure that
275 GH activity led to these differences, AtMAN2's catalytic nucleophile (Wang *et al.*, 2015)
276 was mutated to an alanine (Figs. **2a**, **S3a-c**). AtMAN2^{E335A} had similar fluorescence
277 intensity and subcellular localization to its WT sequence (Fig. **S3d**) but no longer altered
278 mannan content (Fig. **4a**, **S4a**). Similar biochemical changes to the episomal constructs
279 were observed for integrative *AtMAN-mRuby2* constructs driven by a weaker promoter.

After alkaline treatment, the integrative *AtMAN2/5* constructs reduced the content of insoluble mannans (Fig. **S5**), without significant changes in the alkaline-soluble fractions that are rich in mannosylated yeast proteins.

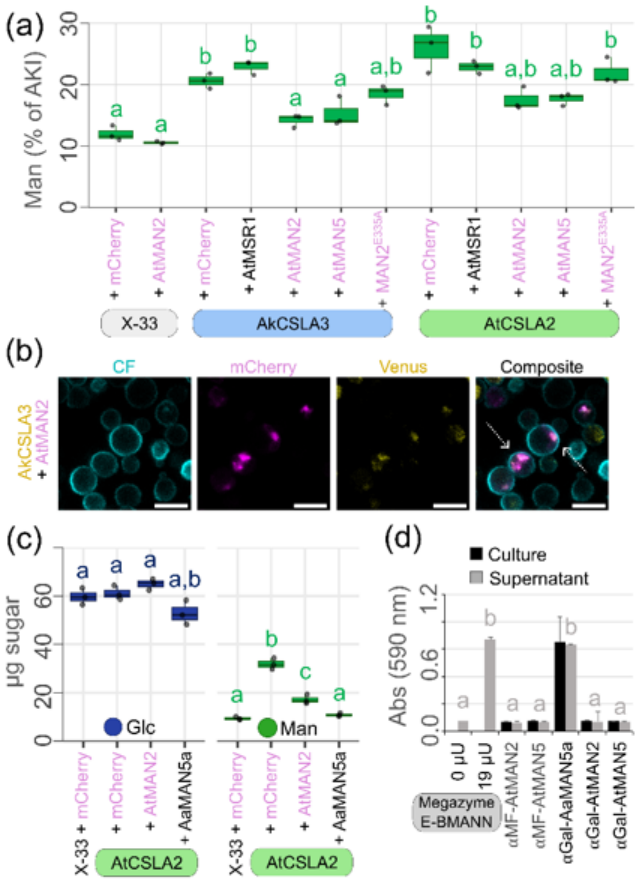

Fig. 4. MAN2/5 enzymes reduce insoluble mannan content in yeast. (a) Relative Man content of insoluble yeast polymers. Box plots show three biological replicates. (b) Arrows mark the co-localization of AkCSLA3-Venus and AtMAN2/5-mCherry and counterstained with CF in confocal micrographs acquired with an 86x (1.2 NA) objective. (c) AKI polymers made by AtCSLA2 plus AtMAN2 or the fungal AaMAN5a. (d) AZCL-galactomannan digestion assays using *Saccharomyces* cell mixtures and supernatant, alongside commercial MAN controls (Megazyme, E-BMANN). Different letters denote significant changes with one-way ANOVA (Tukey's post-hoc test, $P < 0.01$). Magenta labels indicate a C-terminal protein fusion to mCherry. Bars: (b) 5 µm.

AtMAN2 Co-Localizes with AkCSLA3 and Cannot Digest Extracellular β-Mannans

Since AkCSLA3 tolerates C-terminal fluorescent tags (Grieß-Osowski *et al.*, 2025), we co-expressed AtMAN2-mCherry with AkCSLA3-Venus in *Pichia* cells. Although only a subset of AkCSLA3-Venus cells showed mCherry fluorescence due to the greater heterogeneity of episomal plasmid expression, the two proteins co-localized in the endomembrane system (Fig. **4b**, **S4c,d**). Furthermore, AkCSLA3-Venus fluorescence remained constant with either mCherry or MAN-mCherry protein (Fig. **S4c**). We hypothesized that unbranched glucomannan production by CSLAs would perturb yeast cell ultrastructure, and that AtMAN2/5 enzymes could alleviate such defects. However,

293 transmission electron micrographs of 3-day-old *Pichia* cells showed enlarged vacuoles and
294 signs of autophagy, even without CSLAs (Fig. **S7a,b**). Although the same harvest
295 timepoint was suitable for live cell imaging and biochemical analyses in this study and
296 prior work (Grieß-Osowski *et al.*, 2025), we could not observe Golgi bodies in thin sections
297 (100 nm) of cells preserved via high-pressure freezing or chemical fixation. However, we
298 noticed that AkCSLA3 cells (accumulating glucomannan) had 30% thicker cell walls
299 compared to the negative control (**Fig. S7c,d**). Co-expression of AkCSLA3 with the wild-
300 type AtMAN2 (but not the AtMAN2^{E335A} variant) restored the wild-type thickness.

301 Plant MANs are reported to have low catalytic activity (Wang *et al.*, 2015) relative
302 to microbial MANs (Ishii *et al.*, 2016), such as *AaMAN5a* from the plant pathogen
303 *Aspergillus aculeatus*. While AtMAN2 reduced insoluble Man levels in the *Pichia*
304 AtCSLA2 strain by 46%, fungal AaMAN5a led to a 66% decrease (Fig. **4c**), resulting in
305 WT-like yeast cell walls. Since AaMAN5a has been used to ferment β-mannans in
306 *Saccharomyces cerevisiae* (Ishii *et al.*, 2016), we also introduced *AtMANs* in this host and
307 tested their ability to digest exogenous Azurine Cross-Linked (AZCL)-galactomannan.
308 Blue-dyed β-mannan oligosaccharides were released by the supernatant fraction of cells
309 secreting AaMAN5a (Fig. **4d**), or by minute amounts of a fungal MAN purified from
310 *Aspergillus niger*. Neither AtMAN2 nor AtMAN5 could digest extracellular
311 galactomannan (Fig. **4d**), despite replacing their N-terminal transmembrane regions (Fig.
312 **S3a**) with the yeast α-galactosidase (αGal; enabling AaMAN5a secretion) or the α-mating
313 factor (αMF) signal peptide. This is likely due to a lack of AtMAN protein secretion,
314 because fluorescently tagged AtMAN2/5 proteins were retained inside *Pichia* cells despite
315 the addition of the αMF signal peptide (Fig. **S3d**) or if their transmembrane domains were
316 simply removed (Fig. **S4b**). However, when removing the first 34 amino acids without
317 adding a signal peptide, MAN2(34)-mRuby2 proteins became cytosolic and no longer
318 altered the production of insoluble mannans (Fig. **S6a,b**), which occurs in the Golgi lumen.

319 **Tracking Mannan Accumulation and Hemicellulose Solubility**

320 To further quantify how AtMANs influence hemicellulose accumulation in yeast,
321 we applied a novel, genetically encoded probe featuring a carbohydrate-binding module

322 (CBM) derived from a microbial MAN to specifically track β-mannans. The potential
323 utility of CBM-based probes for live cell imaging was previously reviewed (Voiniciuc *et*
324 *al.*, 2018b), and the development of a collection of MannanTrack probes to monitor the
325 activity of mannan synthases in yeast and plants will be fully characterized in a separate
326 manuscript (Robert *et al*, in preparation). Here, we briefly introduce and demonstrate the
327 utility of one MannanTrack probe that consists of the *Podospora anserina* CBM35, which
328 is involved in mannan-binding based on structural and biochemical analyses (Couturier *et*
329 *al.*, 2013). An N-terminal αMF signal peptide targets the PaCBM35 for secretion, and a C-
330 terminal tags containing mScarlet-I (Bindels *et al.*, 2017) and a superfolder mTurquoise2
331 ox (Meiresonne *et al.*, 2019) as ratiometric reporters for red and blue fluorescence (Fig.
332 **5a**). The two fluorescent proteins are separated by a "self-cleaving" P2A linker from the
333 porcine teschovirus-1 2A, which can result in ribosome skipping during translation to
334 generate separate polypeptides from bi-cistronic vectors (Liu *et al.*, 2017). We observed
335 successful skipping and recommencement of translation for our MannanTrack probe
336 resulting in two separatee fluorescent reporters: the mannan-binding αMF-PaCBM35-
337 mScarlet was fully secreted from *Pichia* cells without AkCSLA3 (**Fig. 5a,** additional
338 images in **Fig. S8**), while the mTurquoise2 (downstream of P2A) remained in the cytosol.

339 In contrast to yeast cells with native polysaccharide composition, the αMF-
340 PaCBM35-mScarlet probe was largely retained inside cells (ie. reducing the RFP secretion)
341 producing insoluble mannan (Fig. **5a,b**) and co-localized with AkCSLA3-Venus (Figs. **5a**,
342 **S8**). Based on plate reader measurements (Fig. **5b**), confocal microscopy (Fig. **S8**), and
343 flow cytometry (Fig. **5c**), the introduction of *MAN2/5* significantly increased MannanTrack
344 secretion. For instance, *MAN2/5* enhanced mScarlet fluorescence in the culture supernatant
345 by 20% relative to empty vector or $MAN2^{E335A}$ controls (Fig. **5b**), which prompted us to
346 evaluate β-mannan solubility. Using hot water to directly extract soluble β-1,4-linked
347 glucans from ground yeast cells (Cocuron *et al.*, 2007), we isolated 30–60% more Man
348 from cells co-expressing *AkCSLA3* with *AtMAN2*/5, compared to *AkCSLA3* alone or the
349 non-functional $MAN2^{E335A}$ (Fig. **5d, S9**). To determine whether MANs function similarly
350 in Arabidopsis, we ground dry seeds and isolated alcohol-insoluble residue (AIR) as well
351 as water-soluble fractions for HPAEC-PAD analysis (see extraction scheme in **Fig. S9**).

352 The *man2 man5* mutants contained significantly less Man in both fractions compared to
353 WT, and *CSLA2* overexpression increased Man content primarily in the insoluble polymer
354 fraction (Fig. **5e**). Therefore, we propose that MAN enzyme activity in the endomembrane
355 system converts insoluble mannan polysaccharides into shorter and more hydrophilic
356 molecules.

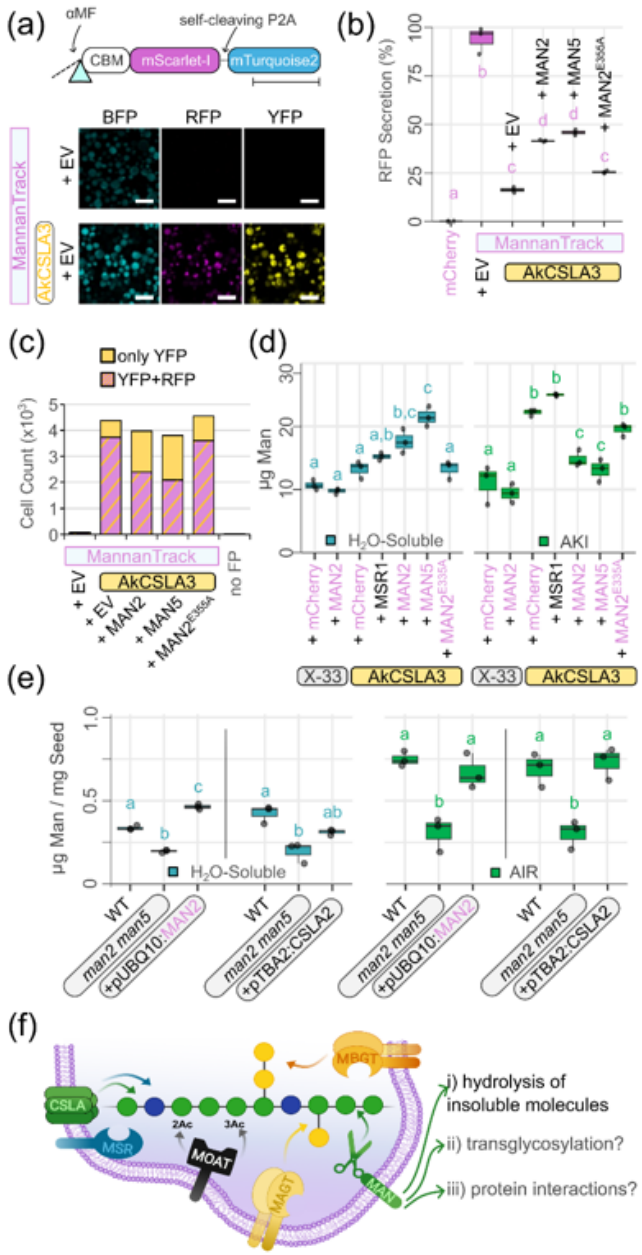

Fig. 5. *MAN2* and *MAN5* promote mannan solubility and secretion. (a) MannanTrack probe components in *Pichia* control strains to validate the blue (BFP), yellow (YFP) and red (RFP) protein fluorescence patterns. (b) Relative secretion (supernatant RFP / cell mixture RFP) of the PaCBM35-mScarlet, normalized to the BFP cell fluorescence relative to empty vector (EV). (c) Number of cells with detectable AkCSLA3-Venus and PaCBM35a-mScarlet fluorescence quantified via flow cytometry. (d) Man content of hot water (H_2O-soluble) and AKI polymers in *Pichia* extracts. (e) Man content of hot water (H_2O-soluble) and AIR polymers in Arabidopsis ground seeds. Box plots show three biological replicates and different letters denote significant changes with one-way ANOVA (Tukey's post-hoc test, $P < 0.01$). Magenta labels indicate a C-terminal protein fusion to mCherry. (f) Updated model of β-mannan biosynthesis in the Golgi apparatus (based on Voiniciuc, 2022) with AtMAN2/5 role(s). Bars: (a) 5 µm.

357

358 **Discussion**

359 **Breaking A Few Bricks to Build a Wall?**

360 Thus far, plant MANs are reported to degrade or cut-and-paste extracellular β-mannans
361 (Bewley, 1997; Moreira & Filho, 2008; Schröder *et al.*, 2009), and typically have
362 antagonistic consequences to Golgi-localized (gluco)mannan synthases (Voiniciuc, 2023).
363 In this study, we discovered that Arabidopsis seeds have reduced mannan production
364 without *MAN2* and *MAN5* (Fig. **1d**, **2c, 5e**), despite wild-type *CSLA2* and *MUCI10*
365 transcript levels (**Fig. 1b**). The significant loss of mannan accumulation in seeds (**Fig. 5e**)
366 despite the normal secretion of other mucilage polysaccharides (**Fig. S1d,e**) implies that
367 *man2 man5* double mutants primarily disrupt mannan elongation. Therefore, we
368 hypothesize that intracellular MAN2/5 enzymes cooperate with Golgi-localized GTs to
369 sustain mannan production (**Fig. 5f**). Although this represents a novel role for endo-MANs,
370 an endo-glucanase is known to participate in cellulose biosynthesis. KORRIGAN1
371 (KOR1) is a plasma membrane-localized cellulase that associates with the Cellulose
372 Synthase Complex (Vain *et al.*, 2014). While genetic studies demonstrate its importance
373 for cellulose synthesis, KOR1's precise mode of action remains elusive. For instance,
374 KOR1 is proposed to relieve mechanical stress placed on the cell as crystalline polymers
375 are deposited into the wall (Mielke *et al.*, 2021). Since unbranched β-mannans also form
376 crystalline structures as they elongate (Grimaud *et al.*, 2019), MAN2/5 could be needed to
377 reduce intracellular polymer aggregates and mechanical strain (Fig. **5f**). This raises the
378 question: why would plant cells build polysaccharides only to immediately degrade them?
379 One possible explanation is that CSL polysaccharide synthases may lack an intrinsic
380 mechanism to stop polymer elongation, making controlled cleavage by GHs essential for
381 regulating fiber length and preventing aggregation.

382 Although *AtCSLA2* overexpression using *pTBA2* forced the elongation of mannans,
383 it could not fully restore the content of water-soluble mannans in seeds (**Fig. 5e**) and
384 disrupted the organization of other mucilage polymers (**Fig. 3a,b**, **S2a,d**). In the *csla2*
385 background, *pTBA2:CSLA2* nearly doubled the amount of mannan compared to WT plants
386 (**Fig. 3c)**. In contrast, *pTBA2:CSLA2* increased the mannan content of *man2 man5* mucilage
387 extracts only to WT levels but significantly disrupted the release of pectin (**Fig. 3d, S2**).

388 The *man2 man5* + *CSLA2* seeds could have reduced secretion of rhamnogalacturonan-I to
389 the cell wall and/or impaired mucilage release due to altered matrix composition and
390 elevated content of birefringent polymers. The second option appears more likely as the
391 SEM of *man2 man5* seeds resembled the WT (Fig. **S1d**), instead of the severe defects of
392 seeds deficient in pectin synthesis (Voiniciuc *et al.*, 2018a). Mutants such as *mum2* are
393 known to release minimal mucilage due to elevated polysaccharide cross-linking rather
394 than a reduction in pectin content (Dean *et al.*, 2007; Voiniciuc *et al.*, 2015c). Therefore,
395 our results reinforce the importance of mannans for matrix polysaccharide architecture as
396 well as cellulose deposition (Voiniciuc *et al.*, 2015b; Yu *et al.*, 2018; Voiniciuc, 2022).
397 MAN2/5 also have functions beyond the seed coat, with similar biosynthetic roles proposed
398 by an independent study of *man2 man5* xylem vessels (Kikuchi *et al.*, 2025). We also found
399 that *man2 man5* double mutants had delayed germination (Fig. **2c**), consistent with *MAN*
400 gene expression in the endosperm (Iglesias-Fernández *et al.*, 2011).

401 **How Hemicellulose Structure Impacts Matrix Polysaccharide Secretion**

402 Despite increasing similarities between branched β-mannan and xyloglucan
403 biosynthesis (Yu *et al.*, 2022; Grieß-Osowski & Voiniciuc, 2023), major questions remain
404 about the precise functions of different hemicellulose structures in plants (Boerjan *et al.*,
405 2024). Xyloglucan mutants lacking Gal decorations have severe growth penalties and
406 secretion defects (Hoffmann & McFarlane, 2024), yet mutations in the five *CSLC* glucan
407 synthases in Arabidopsis leads to relatively mild defects (Kim *et al.*, 2020). Similarly,
408 poplar *csla* mutants lacking detectable mannans in the xylem were shown to grown
409 normally (Guevara-Rozo *et al.*, 2025). We anticipate that galactosylation and/or
410 acetylation are critical substitutions to maintain β-mannan solubility in the Golgi and
411 matrix polysaccharide secretion to the cell wall. The lack of enzymes or donor substrates
412 for mannan or glucan substitution in native *Pichia* cells could explain the intracellular
413 retention of the MannanTrack probe in glucomannan-producing yeast cells (Fig. **5a-c**, **S8**).
414 The modularity of this platform offers further opportunities to decipher how plant GTs and
415 GHs cooperate to define hemicellulose content and properties.
416

417 **Unraveling CSLA and MAN Roles through Yeast Synthetic Biology**

418 While *in vitro* GH assays yield useful catalytic benchmarks and are helpful to
419 improve enzymes for industrial use (Jacobson *et al.*, 2024), they could not have predicted
420 the unexpected biological roles of AtMAN2/5. Yeast species, including *Pichia* and
421 *Saccharomyces* (Grieß-Osowski *et al.*, 2025), can serve as surrogate hosts to characterize
422 plant carbohydrate-active enzymes (Pauly *et al.*, 2019). Intracellular MAN2/5 enzymes
423 reduced insoluble β-mannan production by CSLAs through a variety of biochemical and
424 microscopic assays (Fig. **4**, **5**). Surprisingly, yeast cells showed no evidence of MAN2/5
425 secretion even when the transmembrane domains were replaced with αMF or αGal
426 secretion signals that worked for the MannanTrack probe and the fungal AaMAN5a
427 enzyme (Figs. **4d**, **S3**, **S4**). Previously, MAN2 was affinity purified from *Pichia* cultures
428 for *in vitro* assays using a similar N-terminal truncation (Wang *et al.*, 2015); however, our
429 experiments differ in the choice of the recombinant protein tags and our application of the
430 stronger *pCAT1* promoter in episomal vectors (Vogl *et al.*, 2016). Recent examples of
431 human GTs involved in *N*-glycosylation indicate that the N-terminal transmembrane stem
432 as well as the carbohydrate-active domains can define Golgi localization (Yagi *et al.*,
433 2024). Amino acids beyond the predicted N-terminal membrane stem may thus contribute
434 to the intracellular retention of MAN2/5 in yeast, although the truncation of the first 34
435 AtMAN2 amino acids were sufficient for its redistribution to the cytosol (Fig. **S6**), where
436 it could no longer reduce the accumulation of insoluble mannans. The co-expression of
437 AtMAN2/5 with CSLA elevated the content of water-soluble Man (Fig. **5d**), likely
438 representing β-mannan oligosaccharides isolated from the endomembrane system. Using
439 the same extraction method, *CSLC4* expression in *Pichia* produced water-soluble β-1,4-
440 linked glucan oligosaccharides with an estimated length of four to six residues (Cocuron
441 *et al.*, 2007), while co-expression with *XXT1* (a xylosyltransferase enzyme belonging to
442 the GT34 family that includes *MUCI10/MAGT1*) boosted insoluble glucan production
443 (Robert *et al.*, 2021).
444

445 **Potential Modes of Action for Golgi-Localized MANs**

446 Finally, we consider three (not mutually exclusive) mechanisms by which MAN2/5
447 enzymes could function together with CSLAs to benefit β-mannan synthesis (Fig. **5f**): i)

448 hydrolysis of insoluble molecules, ii) transglycosylation of oligosaccharides, and/or iii)
449 protein interactions with CSLAs. In our yeast data, MAN2/5 enzymes partly hydrolyzed
450 insoluble mannans made by CSLAs (Fig. **4a, 5d**), so we favor the first hypothesis.
451 Transglycosylation, the second mode of action, seems unlikely because purified MAN2
452 enzyme acted solely as a hydrolase *in vitro* (Wang *et al.*, 2015). Cellulose synthases and
453 KORRIGAN1 are known to interact (Vain *et al.*, 2014), so future studies could investigate
454 if CSLAs and MANs form protein complexes in the Golgi apparatus. Nevertheless, the
455 catalytically inactive AtMAN2^{E355A} largely lost its hydrolytic effects despite having no
456 obvious changes in protein expression level or subcellular localization (Figs. **S3**, **S4**), and
457 therefore its potential for interactions with CSLA. Since crops have close orthologs of
458 AtMAN2/5, the unexpected roles of intracellular MANs in CSLA-driven hemicellulose
459 biosynthesis open up new paths to go glyco (Voiniciuc, 2023) and to enhance β-mannan
460 fibers for the bioenergy and bioproducts. Even for plant MANs with characterized
461 biochemical activities, experimental evidence for their subcellular localization is lacking
462 (Table **S8**). Therefore, we anticipate that co-expressing CSLAs with intracellular MANs
463 could alleviate historic bottlenecks to bioengineering plants with designer β-mannans.

464 **Acknowledgments**

465 We thank the following individuals for their technical assistance: Bo Yang (initial *man2*
466 *man5* screening), Hannah Zheng (seed phenotyping), and Karen Kelley (sample
467 preparation at the University of Florida ICBR Electron Microscopy Core Facility,
468 RRID:SCR_019146). Sylvestre Marillonnet provided expert advice and materials for Plant
469 MoClo assembly. Doug Smith and Mariza Miranda provided technical advice for confocal
470 microscopy and flow cytometry at the University of Florida ICBR Cytometry Core Facility,
471 RRID:SCR_019119. This work was supported by startup funding from UF/IFAS, the
472 Horticultural Sciences Department, and the USDA National Institute of Food and
473 Agriculture, Research Capacity Fund (Hatch) project 7004470. CV was also supported by
474 core funding (Leibniz Association) from the Federal Republic of Germany and the state of
475 Saxony-Anhalt, and by DFG grants (414353267). TJ and ME thank the PMCB program
476 and College of Agricultural and Life Sciences (CALS) Dean's Awards for graduate
477 research funding. The research visit of MR was supported by a DAAD (German Academic

Exchange Service) scholarship, while JM was supported by the UF University Scholars program. Finally, we thank Toshihisa Kotake for helpful discussions about MAN function since learning about our independent approaches in the summer of 2024.

Competing Interest Statement: The authors declare no competing interest.

Author Contributions: TJ and CV designed the work, analyzed data and wrote the manuscript. TJ acquired most of the data, with additional contributions from ME, MQ and JM. MR and CV developed the MannanTrack yeast strain.

Data availability

Data supporting the findings of this work are available in the main text and in the figures and tables in Supporting Information. The genetic materials generated in this current study are available from the corresponding author upon request. Popular plasmids and seeds will be donated to Addgene and ABRC, respectively. High-resolution transmission electron micrographs for yeast are on FigShare: dx.doi.org/10.6084/m9.figshare.30369646

References

Berendzen K, Searle I, Ravenscroft D, Koncz C, Batschauer A, Coupland G, Somssich IE, Ülker B. **2005**. A rapid and versatile combined DNA/RNA extraction protocol and its application to the analysis of a novel DNA marker set polymorphic between Arabidopsis thaliana ecotypes Col-0 and Landsberg erecta. *Plant Methods* **1**: 4.

Bewley JD. **1997**. Breaking down the walls — a role for endo-β-mannanase in release from seed dormancy? *Trends in Plant Science* **2**: 464–469.

Bindels DS, Haarbosch L, van Weeren L, Postma M, Wiese KE, Mastop M, Aumonier S, Gotthard G, Royant A, Hink MA, *et al.* 2017. mScarlet: a bright monomeric red fluorescent protein for cellular imaging. *Nature Methods* **14**: 53–56.

Boerjan W, Burlat V, Cosgrove DJ, Dunand C, Dupree P, Haas KT, Ingram G, Jamet E, Mohnen D, Moussu S, *et al.* 2024. Top five unanswered questions in plant cell surface research. *The Cell Surface* **11**: 100121.

Bolle C, Huep G, Kleinbölting N, Haberer G, Mayer K, Leister D, Weisshaar B. **2013**. GABI-DUPLO: a collection of double mutants to overcome genetic redundancy in Arabidopsis thaliana. *The Plant Journal* **75**: 157–171.

510 **Carrillo-Barral N, Matilla AJ, Rodríguez-Gacio MDC, Iglesias-Fernández R**. **2018**. Mannans and
511 endo-β-mannanase transcripts are located in different seed compartments during Brassicaceae
512 germination. *Planta* **247**: 649–661.

513 **Chen J, Yang L, Gu J, Bai X, Ren Y, Fan T, Han Y, Jiang L, Xiao F, Liu Y, *et al.* 2015**. *MAN 3* gene
514 regulates cadmium tolerance through the glutathione-dependent pathway in *Arabidopsis*
515 *thaliana*. *New Phytologist* **205**: 570–582.

516 **Cocuron J-C, Lerouxel O, Drakakaki G, Alonso AP, Liepman AH, Keegstra K, Raikhel N,**
517 **Wilkerson CG**. **2007**. A gene from the cellulose synthase-like C family encodes a β-1,4 glucan
518 synthase. *Proceedings of the National Academy of Sciences* **104**: 8550–8555.

519 **Couturier M, Roussel A, Rosengren A, Leone P, Stålbrand H, Berrin J-G**. **2013**. Structural and
520 Biochemical Analyses of Glycoside Hydrolase Families 5 and 26 β-(1,4)-Mannanases from
521 Podospora anserina Reveal Differences upon Manno-oligosaccharide Catalysis *. *Journal of*
522 *Biological Chemistry* **288**: 14624–14635.

523 **De Farias ET, Da Silva EAA, Toorop PE, Bewley JD, Hilhorst HWM**. **2015**. Expression studies in
524 the embryo and in the micropylar endosperm of germinating coffee (Coffea arabica cv. Rubi)
525 seeds. *Plant Growth Regulation* **75**: 575–581.

526 **Dean GH, Zheng H, Tewari J, Huang J, Young DS, Hwang YT, Western TL, Carpita NC, McCann**
527 **MC, Mansfield SD, *et al.* 2007**. The Arabidopsis MUM2 Gene Encodes a β-Galactosidase
528 Required for the Production of Seed Coat Mucilage with Correct Hydration Properties. *The Plant*
529 *Cell* **19**: 4007–4021.

530 **Downie B, Hilhorst HWM, Bewley JD**. **1997**. Endo-β-mannanase activity during dormancy
531 alleviation and germination of white spruce (*Picea glauca*) seeds. *Physiologia Plantarum* **101**:
532 405–415.

533 **Engler C, Youles M, Gruetzner R, Ehnert T-M, Werner S, Jones JDG, Patron NJ, Marillonnet S**.
534 **2014**. A Golden Gate Modular Cloning Toolbox for Plants. *ACS Synthetic Biology* **3**: 839–843.

535 **Grieß-Osowski A, Robert M, Qiande M, Clauss S, Voiniciuc C**. **2025**. Illuminating Glucomannan
536 Synthases To Explore Cell Wall Synthesis Bottlenecks. *ACS Synthetic Biology* **14**: 2472–2479.

537 **Grieß-Osowski A, Voiniciuc C**. **2023**. Branched mannan and xyloglucan as a dynamic duo in plant
538 cell walls. *The Cell Surface* **9**: 100098.

539 **Griffiths JS, Šola K, Kushwaha R, Lam P, Tateno M, Young R, Voiniciuc C, Dean G, Mansfield SD,**
540 **DeBolt S, *et al.* 2015**. Unidirectional Movement of Cellulose Synthase Complexes in Arabidopsis
541 Seed Coat Epidermal Cells Deposit Cellulose Involved in Mucilage Extrusion, Adherence, and Ray
542 Formation. *Plant Physiology* **168**: 502–520.

543 **Grimaud F, Pizzut-Serin S, Tarquis L, Ladevèze S, Morel S, Putaux J-L, Potocki-Veronese G**.
544 **2019**. *In Vitro* Synthesis and Crystallization of β-1,4-Mannan. *Biomacromolecules* **20**: 846–853.

545 **Guevara-Rozo S, de Vries L, Yoshimi Y, Eli E, Dupree P, Mansfield SD**. **2025**. Unraveling mannan
546 biosynthesis in poplar and spruce: functional characterization of Cellulose Synthase-Like family A
547 (CSLA) genes. *New Phytologist* **n/a**: 10.1111/nph.7068.

548 **Hammer Ø, Harper DAT, Ryan PD**. **2001**. PAST: Paleontological statistics software package for
549 education and data analysis. *Palaeontologia Electronica* **4**.

550 **Hoffmann N, McFarlane HE**. **2024**. Xyloglucan side chains enable polysaccharide secretion to the
551 plant cell wall. *Developmental Cell*: S1534580724003848.

552 **Iglesias-Fernández R, Pastor-Mora E, Vicente-Carbajosa J, Carbonero P**. **2020**. A Possible Role of
553 the Aleurone Expressed Gene HvMAN1 in the Hydrolysis of the Cell Wall Mannans of the Starchy
554 Endosperm in Germinating Hordeum vulgare L. Seeds. *Frontiers in Plant Science* **10**: 1706.

555 **Iglesias-Fernández R, Rodríguez-Gacio MC, Barrero-Sicilia C, Carbonero P, Matilla A**. **2011**.
556 Three endo-β-mannanase genes expressed in the micropylar endosperm and in the radicle
557 influence germination of Arabidopsis thaliana seeds. *Planta* **233**: 25–36.

558 **Ishii J, Okazaki F, Djohan AC, Hara KY, Asai-Nakashima N, Teramura H, Andriani A, Tominaga**
559 **M, Wakai S, Kahar P, *et al.* 2016**. From mannan to bioethanol: cell surface co-display of β-
560 mannanase and β-mannosidase on yeast Saccharomyces cerevisiae. *Biotechnology for Biofuels*
561 **9**: 188.

562 **Jacobson T, Edwards M, Voiniciuc C**. **2024**. Sharp solutions to cleave plant fibers. *Current*
563 *Opinion in Biotechnology* **90**: 103219.

564 **Joët T, Laffargue A, Salmona J, Doulbeau S, Descroix F, Bertrand B, Lashermes P, Dussert S**.
565 **2014**. Regulation of galactomannan biosynthesis in coffee seeds. *Journal of Experimental Botany*
566 **65**: 323–337.

567 **Juhász AE, Greff D, Teutsch B, Gede N, Hegyi P, Horváth EM, Deák PÁ, Nyirády P, Ács N, Juhász**
568 **R**. **2023**. Galactomannans are the most effective soluble dietary fibers in type 2 diabetes: a
569 systematic review and network meta-analysis. *The American Journal of Clinical Nutrition* **117**:
570 266–277.

571 **Kikuchi A, Sato E, Yoshimi Y, Takasaki H, Nishigaki N, Atsuzawa K, Kaneko Y, Yamaguchi M,**
572 **Takahashi D, Dupree P, *et al.* 2025**. Atypical endo-β-1,4-mannannases are necessary for normal
573 glucomannan synthesis in Arabidopsis.

574 **Kim S-J, Chandrasekar B, Rea AC, Danhof L, Zemelis-Durfee S, Thrower N, Shepard ZS, Pauly M,**
575 **Brandizzi F, Keegstra K**. **2020**. The synthesis of xyloglucan, an abundant plant cell wall
576 polysaccharide, requires CSLC function. *Proceedings of the National Academy of Sciences* **117**:
577 20316–20324.

578 **Lin-Cereghino J, Wong WW, Xiong S, Giang W, Luong LT, Vu J, Johnson SD, Lin-Cereghino GP**.
579 **2005**. Condensed protocol for competent cell preparation and transformation of the
580 methylotrophic yeast Pichia pastoris. *BioTechniques* **38**: 44–48.

581 **Liu Z, Chen O, Wall JBJ, Zheng M, Zhou Y, Wang L, Ruth Vaseghi H, Qian L, Liu J**. **2017**.
582 Systematic comparison of 2A peptides for cloning multi-genes in a polycistronic vector. *Scientific*
583 *Reports* **7**: 2193.

584 **Marillonnet S, Grützner R**. **2020**. Synthetic DNA Assembly Using Golden Gate Cloning and the
585 Hierarchical Modular Cloning Pipeline. *Current Protocols in Molecular Biology* **130**: e115.

586 **McGee R, Dean GH, Wu D, Zhang Y, Mansfield SD, Haughn GW**. **2021**. Pectin Modification in
587 Seed Coat Mucilage by *In Vivo* Expression of Rhamnogalacturonan-I- and Homogalacturonan-
588 Degrading Enzymes. *Plant and Cell Physiology* **62**: 1912–1926.

589 **Meiresonne NY, Consoli E, Mertens LMY, Chertkova AO, Goedhart J, den Blaauwen T**. **2019**.
590 Superfolder mTurquoise2ox optimized for the bacterial periplasm allows high efficiency in vivo
591 FRET of cell division antibiotic targets. *Molecular Microbiology* **111**: 1025–1038.

592 **Mielke S, Zimmer M, Meena MK, Dreos R, Stellmach H, Hause B, Voiniciuc C, Gasperini D**.
593 **2021**. Jasmonate biosynthesis arising from altered cell walls is prompted by turgor-driven
594 mechanical compression. *Science Advances* **7**: eabf0356.

595 **Moreira LRS, Filho EXF**. **2008**. An overview of mannan structure and mannan-degrading enzyme
596 systems. *Applied Microbiology and Biotechnology* **79**: 165–178.

597 **Naoumkina M, Vaghchhipawala S, Tang Y, Ben Y, Powell RJ, Dixon RA**. **2008**. Metabolic and
598 genetic perturbations accompany the modification of galactomannan in seeds of Medicago
599 truncatula expressing mannan synthase from guar (Cyamopsis tetragonoloba L.). *Plant*
600 *Biotechnology Journal* **6**: 619–631.

601 **Nelson BK, Cai X, Nebenführ A**. **2007**. A multicolored set of *in vivo* organelle markers for co-
602 localization studies in Arabidopsis and other plants. *The Plant Journal* **51**: 1126–1136.

603 **Nonogaki H, Gee OH, Bradford KJ**. **2000**. A Germination-Specific Endo-β-Mannanase Gene Is
604 Expressed in the Micropylar Endosperm Cap of Tomato Seeds. *Plant Physiology* **123**: 1235–1246.

605 **Pauly M, Gawenda N, Wagner C, Fischbach P, Ramírez V, Axmann IM, Voiniciuc C**. **2019**. The
606 Suitability of Orthogonal Hosts to Study Plant Cell Wall Biosynthesis. *Plants* **8**: 516.

607 **Pauly M, Keegstra K**. **2008**. Cell-wall carbohydrates and their modification as a resource for
608 biofuels. *The Plant Journal* **54**: 559–568.

609 **Prielhofer R, Barrero JJ, Steuer S, Gassler T, Zahrl R, Baumann K, Sauer M, Mattanovich D,**
610 **Gasser B, Marx H**. **2017**. GoldenPiCS: a Golden Gate-derived modular cloning system for applied
611 synthetic biology in the yeast Pichia pastoris. *BMC Systems Biology* **11**: 123.

612 **Ralet M-C, Crépeau M-J, Vigouroux J, Tran J, Berger A, Sallé C, Granier F, Botran L, North HM**.
613 **2016**. Xylans Provide the Structural Driving Force for Mucilage Adhesion to the Arabidopsis Seed
614 Coat. *Plant Physiology* **171**: 165–178.

615 **Robert M, Waldhauer J, Stritt F, Yang B, Pauly M, Voiniciuc C**. **2021**. Modular biosynthesis of
616 plant hemicellulose and its impact on yeast cells. *Biotechnology for Biofuels* **14**: 140.

617 **Rodríguez-Gacio MDC, Iglesias-Fernández R, Carbonero P, Matilla ÁJ**. **2012**. Softening-up
618 mannan-rich cell walls. *Journal of Experimental Botany* **63**: 3975–3988.

619 **Scheller HV, Ulvskov P**. **2010**. Hemicelluloses. *Annual Review of Plant Biology* **61**: 263–289.

620 **Schindelin J, Arganda-Carreras I, Frise E, Kaynig V, Longair M, Pietzsch T, Preibisch S, Rueden C,**
621 **Saalfeld S, Schmid B, *et al.* 2012**. Fiji: an open-source platform for biological-image analysis.
622 *Nature Methods* **9**: 676–682.

623 **Schröder R, Atkinson RG, Redgwell RJ**. **2009**. Re-interpreting the role of endo-β-mannanases as
624 mannan endotransglycosylase/hydrolases in the plant cell wall. *Annals of Botany* **104**: 197–204.

625 **Thorne K, Urbanowicz BR, Hahn MG**. **2023**. Plant Cell Wall Glycan-Directed Monoclonal
626 Antibodies. In: Plant Cell Walls. Boca Raton: CRC Press, 206–236.

627 **Vain T, Crowell EF, Timpano H, Biot E, Desprez T, Mansoori N, Trindade LM, Pagant S, Robert S,**
628 **Höfte H, *et al.* 2014**. The Cellulase KORRIGAN Is Part of the Cellulose Synthase Complex. *Plant*
629 *Physiology* **165**: 1521–1532.

630 **Vogl T, Sturmberger L, Kickenweiz T, Wasmayer R, Schmid C, Hatzl A-M, Gerstmann MA, Pitzer**
631 **J, Wagner M, Thallinger GG, *et al.* 2016**. A Toolbox of Diverse Promoters Related to Methanol
632 Utilization: Functionally Verified Parts for Heterologous Pathway Expression in Pichia pastoris.
633 *ACS Synthetic Biology* **5**: 172–186.

634 **Voiniciuc C**. **2017**. Whole-seed Immunolabeling of Arabidopsis Mucilage Polysaccharides. *BIO-*
635 *PROTOCOL* **7**: 1–10.

636 **Voiniciuc C**. **2022**. Modern mannan: a hemicellulose's journey. *New Phytologist* **234**: 1175–1184.

637 **Voiniciuc C**. **2023**. It's time to go glyco in cell wall bioengineering. *Current Opinion in Plant*
638 *Biology* **71**: 102313.

639 **Voiniciuc C, Dama M, Gawenda N, Stritt F, Pauly M**. **2019**. Mechanistic insights from plant
640 heteromannan synthesis in yeast. *Proceedings of the National Academy of Sciences* **116**: 522–
641 527.

642 **Voiniciuc C, Engle KA, Günl M, Dieluweit S, Schmidt MH-W, Yang J-Y, Moremen KW, Mohnen**
643 **D, Usadel B**. **2018a**. Identification of Key Enzymes for Pectin Synthesis in Seed Mucilage. *Plant*
644 *Physiology* **178**: 1045–1064.

645 **Voiniciuc C, Günl M**. **2016**. Analysis of Monosaccharides in Total Mucilage Extractable from
646 Arabidopsis Seeds. *BIO-PROTOCOL* **6**: 1–12.

647 **Voiniciuc C, Günl M, Schmidt MH-W, Usadel B, Guenl M, Schmidt MH-W, Usadel B**. **2015a**.
648 Highly Branched Xylan Made by IRREGULAR XYLEM14 and MUCILAGE-RELATED21 Links Mucilage
649 to Arabidopsis Seeds. *Plant Physiology* **169**: 2481–95.

650 **Voiniciuc C, Pauly M, Usadel B**. **2018b**. Monitoring polysaccharide dynamics in the plant cell
651 wall. *Plant Physiology* **176**: 2590–2600.

652 **Voiniciuc C, Schmidt MH-W, Berger A, Yang B, Ebert B, Scheller HV, North HM, Usadel B, Günl**
653 **M**. **2015b**. MUCILAGE-RELATED10 Produces Galactoglucomannan That Maintains Pectin and
654 Cellulose Architecture in Arabidopsis Seed Mucilage. *Plant Physiology* **169**: 403–420.

655 **Voiniciuc C, Yang B, Schmidt MH-W, Günl M, Usadel B**. **2015c**. Starting to gel: how Arabidopsis
656 seed coat epidermal cells produce specialized secondary cell walls. *International Journal of*
657 *Molecular Sciences* **16**: 3452–3473.

658 **Voiniciuc C, Zimmermann E, Schmidt MH-W, Günl M, Fu L, North HM, Usadel B**. **2016**.
659 Extensive Natural Variation in Arabidopsis Seed Mucilage Structure. *Frontiers in Plant Science* **7**.

660 **Vollen K, Zhao C, Alonso JM, Stepanova AN**. **2024**. Sourcing DNA parts for synthetic biology
661 applications in plants. *Current Opinion in Biotechnology* **87**: 103140.

662 **Wang Y, Azhar S, Gandini R, Divne C, Ezcurra I, Aspeborg H**. **2015**. Biochemical characterization
663 of the novel endo-β-mannanase AtMan5-2 from Arabidopsis thaliana. *Plant Science* **241**: 151–
664 163.

665 **Wang A, Wang X, Ren Y, Gong X, Bewley JD**. **2005**. Endo-β-mannanase and β-mannosidase
666 activities in rice grains during and following germination, and the influence of gibberellin and
667 abscisic acid. *Seed Science Research* **15**: 219–227.

668 **Wu Q, Meng YT, Feng ZH, Shen RF, Zhu XF**. **2023**. The endo-beta mannase MAN7 contributes to
669 cadmium tolerance by modulating root cell wall binding capacity in *Arabidopsis thaliana*. *Journal*
670 *of Integrative Plant Biology* **65**: 1670–1686.

671 **Yagi H, Tateo S, Saito T, Ohta Y, Nishi E, Obitsu S, Suzuki T, Seetaha S, Hellec C, Nakano A, *et al.***
672 **2024**. Deciphering the sub-Golgi localization of glycosyltransferases via 3D super-resolution
673 imaging. *Cell Structure and Function* **49**: 47–55.

674 **Yang B, Stamm G, Bürstenbinder K, Voiniciuc C**. **2022**. Microtubule-associated IQD9
675 orchestrates cellulose patterning in seed mucilage. *New Phytologist* **235**: 1096–1110.

676 **Yu L, Lyczakowski JJ, Pereira CS, Kotake T, Yu X, Li A, Mogelsvang S, Skaf MS, Dupree P**. **2018**.
677 The Patterned Structure of Galactoglucomannan Suggests It May Bind to Cellulose in Seed
678 Mucilage. *Plant Physiology* **178**: 1011–1026.

679 **Yu L, Shi D, Li J, Kong Y, Yu Y, Chai G, Hu R, Wang J, Hahn MG, Zhou G**. **2014**. CELLULOSE
680 SYNTHASE-LIKE A2, a Glucomannan Synthase, Is Involved in Maintaining Adherent Mucilage
681 Structure in Arabidopsis Seed. *Plant Physiology* **164**: 1842–1856.

682 **Yu L, Yoshimi Y, Cresswell R, Wightman R, Lyczakowski JJ, Wilson LFL, Ishida K, Stott K, Yu X,**
683 **Charalambous S, *et al.* 2022**. Eudicot primary cell wall glucomannan is related in synthesis,
684 structure and function to xyloglucan. *The Plant Cell*: koac238.

685 **Zhang R, Li B, Zhao Y, Zhu Y, Li L**. **2024**. An essential role for mannan degradation in both cell
686 growth and secondary cell wall formation. *Journal of Experimental Botany* **75**: 1407–1420.

687 **Zhong R, Cui D, Ye Z**. **2019**. Evolutionary origin of O-acetyltransferases responsible for
688 glucomannan acetylation in land plants. *New Phytologist* **224**: 466–479.

689

690

691 **Supporting Information**

692

693 Additional Supporting Information may be found online:

694 Methods S1 Supplemental Methods for Plant and Yeast Experiments

695 Fig. S1 Additional phenotyping of *man2 man5* seeds.

696 Fig. S2 Mucilage architecture after *CSLA2* overexpression in the seed coat.

697 Fig. S3 MAN2 and MAN5 protein structure and expression in yeast.

698 Fig. S4 Polymer composition following CSLA/MAN expression in *Pichia*.

699 Fig. S5 Fractionation of alkaline-soluble and insoluble cell wall glycans.

700 Fig. S6 AtMAN2 truncation alters its localization and its hydrolytic effects.

701 Fig. S7 Transmission electron microscopy of *Pichia* cells.

702 Fig. S8 Confocal microscopy of MannanTrack in yeast cells.

703 Fig. S9 Workflow of water-soluble mannan extraction from yeast and plant samples.

704 Table S1 Sequences of primers used for genotyping and quantitative PCR.

705 Table S2 Sequences of primers used for cloning.

706 Table S3 Monosaccharide composition of total mucilage extracts.

707 Table S4 Plant constructs and functional evaluation.

708 Table S5 Yeast strains used in this study.

709 Table S6 Summary of characterized plant MANs.

710 Video S1 Timelapse of Golgi-YFP and MAN2-mCherry in Tobacco

711

Figure Legends

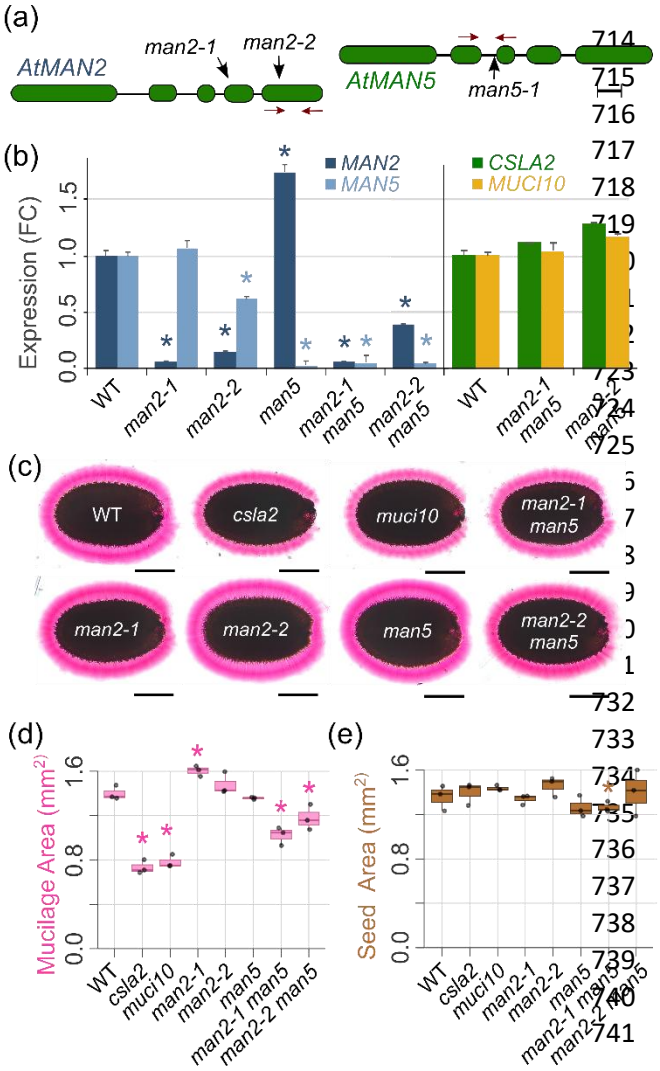

Fig. 1. Mannanase double mutant Arabidopsis seeds have decreased mucilage accumulation. (a) T-DNA insertions in *AtMAN2* and *AtMAN5* genes, showing exon and intron structure. Red arrows indicate positions of primer binding utilized for quantitative PCR (Scale bar, 200 bp). (b) Fold changes in *AtMAN2* and *AtMAN5* or *AtCSLA2* and *AtMUCI10* transcription relative to WT in mature green siliques. Data show mean + SD of three biological replicates normalized to the geometric mean of *UBQ5* and *GAPC1*. Asterisks indicate significant decreases relative to WT (Student's *t* test, $P < 0.01$). (c) Pectin release of WT and mutant seeds stained with RR. (d) Projected mucilage and (e) seed surface area. Data shows mean + SD of three biological replicates (around 20 seeds each). Asterisks indicate significant decreases relative to WT (Student's *t* test, $P < 0.05$). Bars: (c) 200 µm.

742

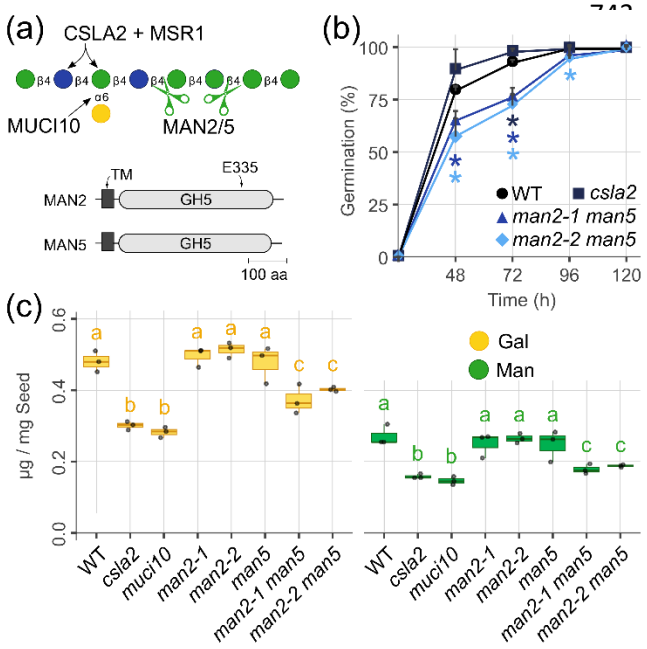

Fig. 2. The *man2 man5* mutant seeds are impaired in β-mannan elongation. (a) Schematic of mucilage mannan biosynthesis and MAN2/5 protein domains. (b) Mean + SD germination rate for three biological replicates. For each time point, asterisks indicate significant decreases relative to WT (Student's *t* test, $P < 0.05$). (c) Absolute monosaccharide levels of three biological replicates. Different letters denote significant changes with one-way ANOVA (Tukey's post-hoc test, $P < 0.01$).

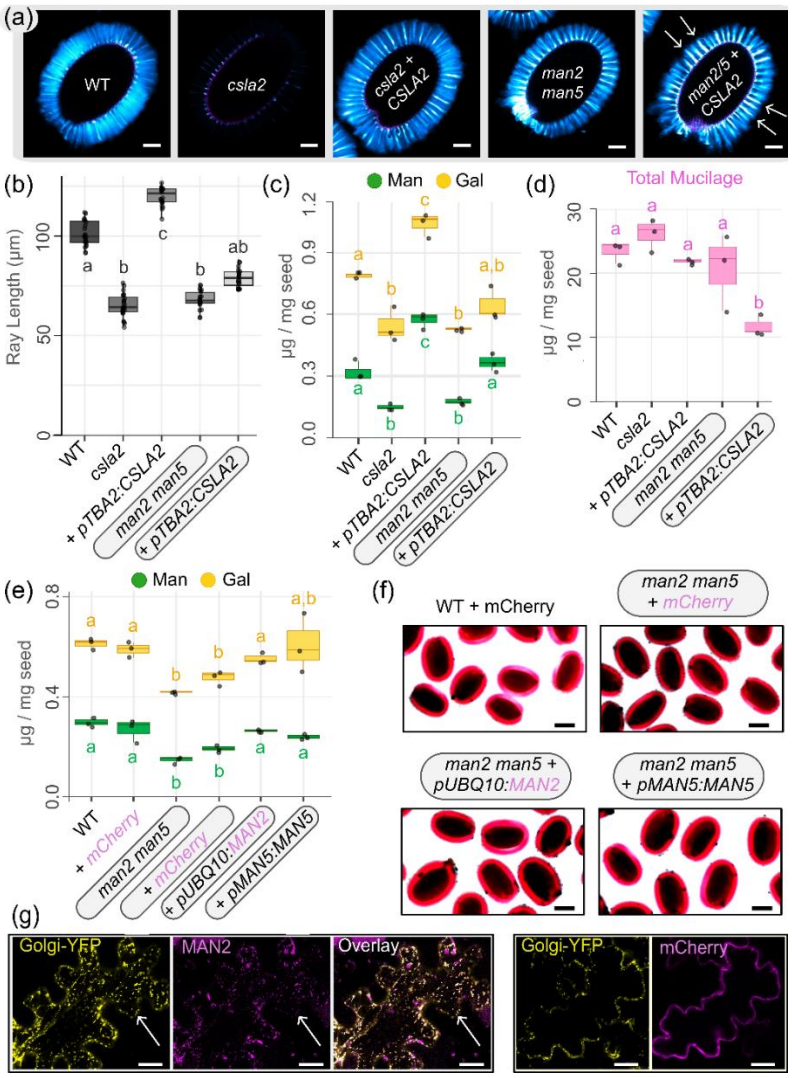

Fig. 3. Golgi-localized MAN enzymes are important for mucilage structure. (a) CF staining of β-glucans in seed mucilage. Arrows mark disordered rays. (b) Length of CF-stained rays. (c) *AtCSLA2* overexpression affects Gal and Man content, and (d) total mucilage release. Biochemical (e) and mucilage RR staining (f) complementation of *man2 man5* by AtMAN gDNA constructs. Different letters denote significant changes with one-way ANOVA (Tukey's post-hoc test, $P < 0.01$). (g) Optical sections of *N. benthamiana* leaves expressing a Golgi-YFP marker and AtMAN2-mCherry or an mCherry control. Arrows mark co-localization. Bars: (a) 100 µm, (f) 200 µm, (g) 30 µm.

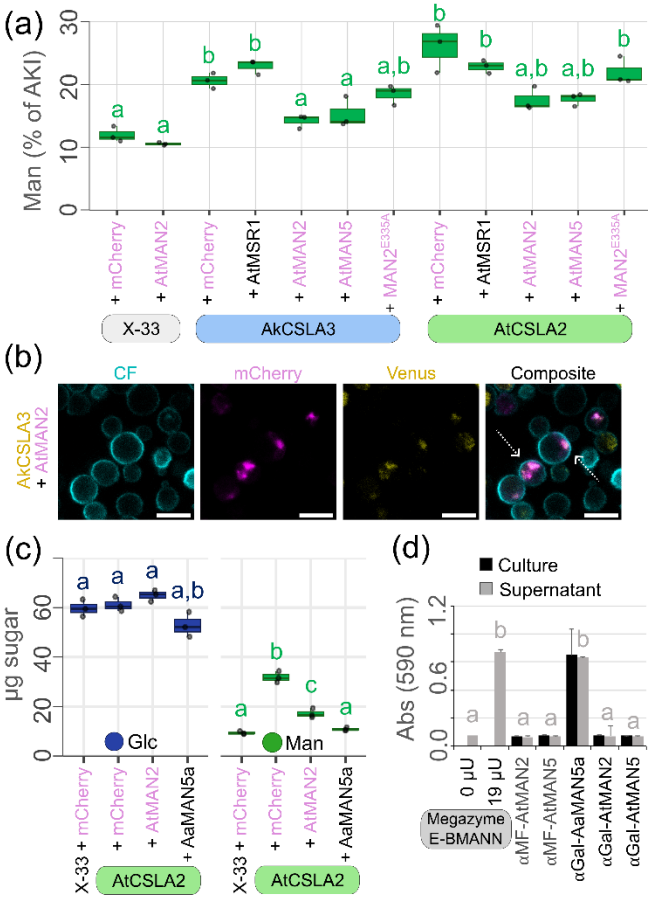

Fig. 4. MAN2/5 enzymes reduce insoluble mannan content in yeast. (a) Relative Man content of insoluble yeast polymers. Box plots show three biological replicates. (b) Arrows mark the co-localization of AkCSLA3-Venus and AtMAN2/5-mCherry and counterstained with CF in confocal micrographs acquired with an 86x (1.2 NA) objective. (c) AKI polymers made by AtCSLA2 plus AtMAN2 or the fungal AaMAN5a. (d) AZCL-galactomannan digestion assays using *Saccharomyces* cell mixtures and supernatant, alongside commercial MAN controls (Megazyme, E-BMANN). Different letters denote significant changes with one-way ANOVA (Tukey's post-hoc test, $P < 0.01$). Magenta labels indicate a C-terminal protein fusion to mCherry. Bars: (b) 5 µm.

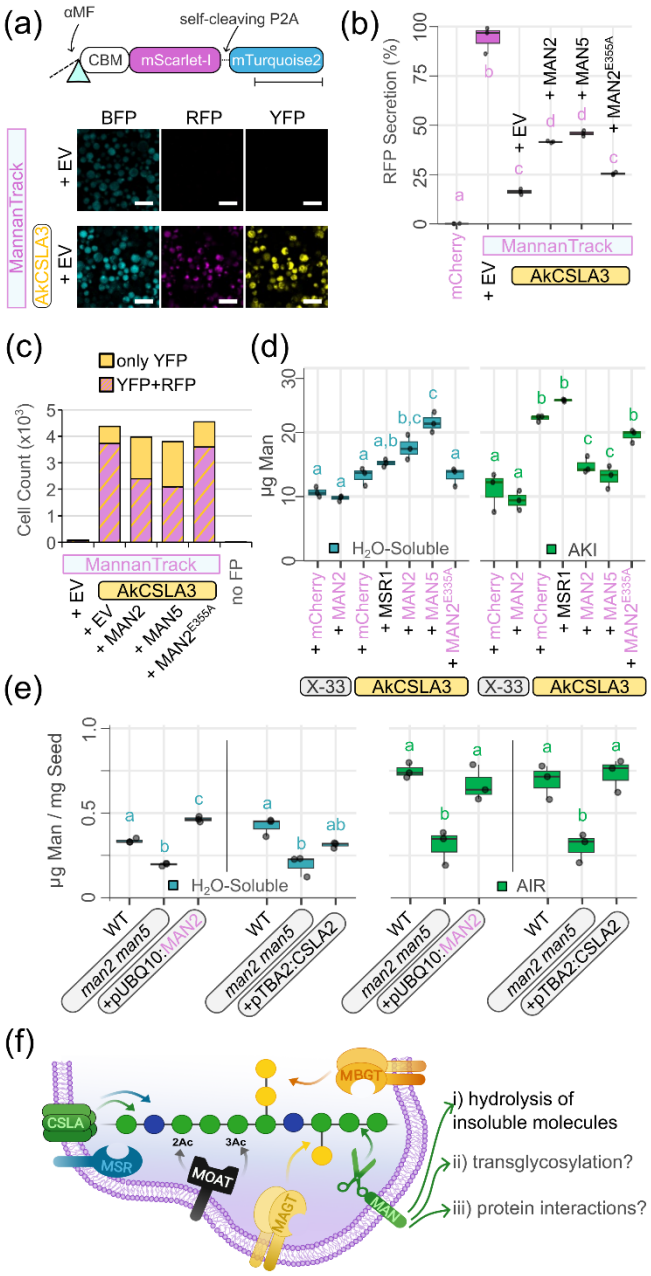

Fig. 5. *MAN2* and *MAN5* promote mannan solubility and secretion. (a) MannanTrack probe components in *Pichia* control strains to validate the blue (BFP), yellow (YFP) and red (RFP) protein fluorescence patterns. (b) Relative secretion (supernatant RFP / cell mixture RFP) of the PaCBM35-mScarlet, normalized to the BFP cell fluorescence relative to empty vector (EV). (c) Number of cells with detectable AkCSLA3-Venus and PaCBM35a-mScarlet fluorescence quantified via flow cytometry. (d) Man content of hot water (H_2O-soluble) and AKI polymers in *Pichia* extracts. (e) Man content of hot water (H_2O-soluble) and AIR polymers in Arabidopsis ground seeds. Box plots show three biological replicates and different letters denote significant changes with one-way ANOVA (Tukey's post-hoc test, $P < 0.01$). Magenta labels indicate a C-terminal protein fusion to mCherry. (f) Updated model of β-mannan biosynthesis in the Golgi apparatus (based on Voiniciuc, 2022) with AtMAN2/5 role(s). Bars: (a) 5 µm.